DNS OF TURBULENT FLOW IN AN ELLIPTICAL DUCT

Nikolay Nikitin
Institute of Mechanics, Moscow State University
1 Michurinsky prospect, 119899 Moscow, Russia
nvnikitin@mail.ru

Alexander Yakhot
Department of Mechanical Engineering
Ben-Gurion University of the Negev
Beersheva 84105, Israel
yakhot@bgu.ac.il

ABSTRACT

Direct numerical simulation (DNS) of fully-developed turbulent flow in elliptical ducts is performed. The mean cross-stream secondary flows exhibited by two counter-rotating vortices which are symmetrical about the major ellipse's axis. The mean flow characteristics and turbulence statistics have been obtained. The variation of the statistical quantities such as the Reynolds stresses and turbulence intensities along the minor axis of the elliptical cross-section were found to be similar to plane channel data. The turbulent statistics along the major axis was found to be inhibited by the secondary flow transferring high-momentum fluid from the duct's center towards the wall. The instantaneous velocity fields in the near-wall region revealed structures similar to the "streaks" except in the vicinity of the major axis endpoints where significant reduction of the turbulent activity due to the wall transverse curvature effect was found.

INTRODUCTION

Direct numerical simulation (DNS) has been recognized as a powerful and reliable tool for studying turbulent flows. Numerous studies showed that results obtained by DNS are in excellent agreement with experimental findings, if they are reliable (Moin and Mahesh, 1998). DNS-based studies are advantageous to experimental methods in that a practically unrestrained, far more detailed study of the flow field structure can be achieved. Another, perhaps even more important advantage is that DNS allows exposure of new important physical mechanisms of turbulence production and self-sustainability. However one major difficulty that arises with a numerical investigation of turbulent flow is the presence of a vast, continuous range of excited scales of motion which must be correctly resolved by numerical simulation. Another principal restriction is that most DNS-based works have focused on simple-geometry flows. For wall-bounded turbulent flows, the majority of successful DNS-based simulations dealt with simple geometry cases such as a pipe and a straight square duct (Gavrilakis, 1992; Huser and Biringen, 1993; Madabhushi and Vanka, 1993; Eggels et al., 1994; Nikitin, 1994; Nikitin, 1997). Discretization of Navier–Stokes equations in the vicinity of complex geometry boundaries is the most difficult problem for numerical simulating flow problems. The use of boundary-fitted, structured or non-structured grids solves this problem, but implementing such grids leads to low-order numerical algorithms which involve high-cost computer time, are memory consuming, and cannot be efficiently used for DNS.

An alternative approach is based on the immersed-boundary (IB) method as introduced by Peskin (1972). IB methods were originally used to reduce the simulation of complex geometry flows to that defined on simple (rectangular) domains. This can be illustrated if we consider a flow of an incompressible fluid around an obstacle Ω (S is its boundary) placed onto a rectangular domain Π. The flow is governed by the Navier–Stokes and incompressibility equations with the no-slip boundary condition on S. The fundamental idea behind IB methods is to describe the flow problem, defined in $\Pi - \Omega$, by solving the governing equations inside an entire rectangular Π *without* an obstacle using simple rectangular (cartesian or cylindrical) meshes, which, generally speaking, do not coincide with the boundary S. To impose the no-slip condition on an obstacle surface S (which becomes an internal surface for the rectangular domain wherein the problem is formulated), a source term $\mathbf{f}$ (an artificial body force) is added to the Navier–Stokes equations. The purpose of the forcing term is to impose the no-slip boundary condition on the $\mathbf{x}_S$-points which define the immersed boundary S.

IB-based approaches differ by the methods used to introduce an artificial force into the governing equations. References of different immersed-boundary methods can be found in Balaras (2004) and Moin (2002). For example, a "direct forcing" approach was suggested by Mohd-Yusof (1997) for numerical schemes using spectral methods. Fadlun et al. (2000) and Kim et al. (2001) developed the idea of "direct forcing" for implementing finite-volume methods on a staggered grid. Kim et al. (2001) contributed two basic advances for introducing direct forcing when using immersed-boundary methods. One was a new numerically stable interpolation procedure for evaluating the forcing term, and the other advance introduced a mass source/sink to enhance the solution's accuracy.

The main advantages of IB methods are that they are based on relatively simple numerical codes and highly effective algorithms, both of which result in considerable reduction of required computing resources. The main disadvantage, however, in using simple computational meshes is the difficulty

in resolving local regions with steep (sharp, abrupt) variation of flow characteristics. These are especially pronounced for high-Reynolds number flows. In addition, in order to impose the boundary conditions, numerical algorithms require that the node velocity values should be interpolated onto the boundary points because the boundary S does not coincide with the gridpoints of a rectangular mesh. Finally, due to the time-stepping algorithms used in "direct forcing" IB methods the no-slip boundary condition is imposed with $O(\Delta t^2)$ accuracy. Therefore, implementation of IB methods to simulate turbulent flows requires careful monitoring to avoid possible contamination of numerical results arising from inaccurate boundary conditions.

Our present study is based on the direct forcing approach suggested by Kim et al. (2001). In this paper, we applied the IB method for DNS of fully-developed turbulent flow in ducts with an elliptical cross-section.[1] An elliptical pipe is a slight modification of a classic pipe and the simplest type of non-circular ducts. To the best of our knowledge, Cain and Duffy (1971) are the only authors to have presented experimental data on turbulent flow in elliptical ducts. As in other non-circular ducts, the flow is peculiar by developing secondary mean motions in the plane perpendicular to the streamwise flow direction known as secondary flows of the Prandtl's second kind, and created by generating the mean streamwise vorticity due to the anisotropy of the Reynolds stresses. Such motions are an intrinsic feature of turbulent flow in non-circular ducts and do not take place in a plane channel or a circular pipe. Despite the fact that the secondary velocity in non-circular ducts is only 1-3% of the streamwise bulk velocity, secondary motions play a significant role by cross-stream transferring momentum, heat and mass (Demuren and Rodi, 1984). The development of turbulent closure models that can reliably predict turbulence-driven secondary flows in non-circular ducts is currently unfeasible due to a lack of detailed experimental data. DNS can provide the necessary data, however reported DNS-based studies only relate to turbulent flow through straight ducts of square cross-section. To the knowledge of the authors, ours is the first study to perform a DNS of turbulent flow in elliptical ducts and to report the results of DNS calculations. Our results support the recent trend to employ immersed-boundary methods formulated on rectangular meshes as a tool for simulating turbulent flows.

NUMERICAL METHOD

We consider an incompressible fluid forced by pressure difference to move through an elliptical duct

$$G = \{(x, y, z) : \quad x^2/a^2 + y^2/b^2 < 1,\ 0 \le z \le L_z\}. \qquad (1)$$

Fully-developed flow in a duct is governed by the Navier–Stokes equations

$$\frac{\partial \mathbf{u}}{\partial t} = -(\mathbf{u}\nabla)\mathbf{u} + \nu\nabla^2\mathbf{u} - \nabla p + \mathbf{k}\frac{\Delta p}{\rho L_z}, \qquad (2)$$

subjected to the incompressibility constraint

$$\nabla \cdot \mathbf{u} = 0, \qquad (3)$$

where $\mathbf{u} = (u_x, u_y, u_z)$ is the velocity field, p is the kinematic pressure, ν is the kinematic viscosity, and $\mathbf{k}$ is the unit vector in the z-direction. We imply the no-slip boundary condition at the wall and periodic boundary conditions in the streamwise z direction. In Eq. (2), we split the pressure gradient into two terms, where, due to the implied periodicity, the first (∇p) does not contribute to the overall pressure drop. In order to maintain a constant flow rate Q_0, the pressure drop is determined by the value of $\Delta p(t)$, which is obtained at each time instant from the constraint

$$\int\int_{\Omega} u_z(x, y, z, t)\mathrm{d}x\mathrm{d}y = Q_0 = \text{const}. \qquad (4)$$

In Eq. (4), Ω denotes the duct's cross-section, and the integral does not depend on z due to incompressibility.

Numerical solution to the system of equations (2-3) was basically obtained by using the IB approach suggested by Kim et al. (2001). The only difference is that instead of using a time-advancement scheme of Rai and Moin (1991) we employed the algorithm suggested in (Nikitin, 1996). Both schemes exploit third order accurate explicit Runge–Kutta methods for convective terms and second order accurate implicit methods for viscous terms; thus, overall accuracy of both schemes is of second-order in time.

Following the IB approach, we solve the governing equations in a three-dimensional computational *rectangular* domain Π

$$\Pi = \{(x, y, z) : \ |x| \le A,\ |y| \le B,\ 0 \le z \le L_z,\ A > a,\ B > b\}, \qquad (5)$$

which includes a duct with an elliptical (but can be, generally speaking, *arbitrary*) cross-section. We used the second-order accurate finite-difference discretization on a rectangular mesh incorporating the concept of staggered grids. The Poisson equation for the pressure is solved by fast direct methods using the fast Fourier transform in the z-direction and the cyclic reduction method in the (x, y)-plane (Swarztrauber, 1974).

The numerical procedure can be described as follows. Starting with some initial three-dimensional velocity field, the governing equations are integrated in time until a statistically steady state is reached. Then the mean flow and turbulence statistical quantities are obtained by further time-advancing and averaging both in time and along the homogeneous z-direction[2]. As a result of this averaging procedure is that the mean fields depend on x and y.

In this paper, the presented results of the calculated velocities and turbulence intensities are normalized by the bulk velocity, U_b. The ellipse's major semiaxis, a, is the characteristic length; $l_\tau = \nu/u_\tau$ and $u_\tau = (\overline{\tau}_w/\rho)^{1/2}$ are the wall length and shear-velocity units, respectively[3]. For the fully-developed flow, the mean wall shear stress, $\overline{\tau}_w$, is balanced by the mean pressure drop, Δp, and defined from

$$\overline{\tau}_w = \Delta p\frac{D_h}{4L_z}, \qquad D_h = \frac{4\Omega}{P_w}, \qquad (6)$$

where D_h is the hydraulic diameter, and Ω and P_w are the duct (ellipse) cross-section area and perimeter length, respectively.

[1] The suggested numerical algorithm can be used for simulating flows in ducts of arbitrary cross-section.

[2] In this paper, $\langle\rangle$ denotes averaging in time and over the streamwise direction. For convenience, an upper case letter Ξ is used for $\Xi \equiv \langle\xi\rangle$. A quantity ξ' means an instantaneous fluctuation of ξ, i.e., $\xi = \langle\xi\rangle + \xi'$.

[3] For ξ^+, the subscript $^+$ denotes that a quantity ξ is normalized by the wall units.

Case	EP2	EP5
b/a	0.67	0.5
D_h/a	1.59	1.30
Re_{2a}	7547	9252
Re_{D_h}	6000	6000
$N_x \times N_y$	200×160	200×160
N_z	256	256
a^+	256	312
b^+	171	156
L_z/D_h	6.0	6.0
L_z^+	2453	2431
$h^+_{x,min}$	1.3	1.6
$h^+_{x,max}$	3.7	4.5
$h^+_{y,min}$	1.1	1.0
$h^+_{y,max}$	3.1	2.8
h_z^+	9.6	9.5
Δ^+_{max}	4.8	4.9
Δt^+	0.37	0.16
CFL	0.69	0.32
$T_{av}u_\tau/a$	60	60

Table 1: Elliptical duct runs parameters.

ELLIPTICAL DUCT: DNS RESULTS

In this paper, geometrical and computational domain parameters are scaled on the length of the ellipse's major semi-axis a. Two elliptical ducts were considered[4]: $b/a = 0.67$ and $b/a = 0.5$. The simulations were carried out for $Re_{D_h} = 6000$, where Re_{D_h} is the Reynolds number based on the bulk velocity U_b and the hydraulic diameter D_h defined in (6). Simulation parameters are summarized in table 1. The wall unit scales are defined by the mean wall shear stress $\overline{\tau}_w$, (6). The cross-stream grid refinement tests were performed in order to exclude possible non-physical contamination of the results due to the employed numerical method. The finest computational mesh includes 8.192×10^6 grid points, 4.84×10^6 of them inside an elliptical duct for cases EP2 and EP5. The size of the smallest computational cell is about one viscous length unit in the domain cross-section and less than 10 viscous lengths in the streamwise direction. The mean grid width is defined as $\Delta^+ = (h_x^+ h_y^+ h_z^+)^{1/3}$.

The length of the computational domain is $L_z/D_h = 6$, and averaging in time and in the axial direction can be considered quite adequate, in particular for the simulations with $T_{av}u_\tau/a \geq 100$. This is because distributions of mean flow properties become symmetric with respect to the ellipse's principal axes[5].

Mean flow properties are summarized in table 2. C_f is the friction coefficient computed from the DNS data and $\Delta(C_f)$ is its relative deviation from the correlation based on Blasius' law when it is applied for non-circular ducts by using the hydraulic diameter

$$C_f = 0.0791 Re_{D_h}^{-0.25}, \quad Re_{D_h} = U_m D_h/\nu. \tag{7}$$

Figure 1 shows the mean streamwise velocity U_z contours for wide and narrow pipes. The corresponding values of U_c/U_b are 1.29 and 1.27. The cross-stream mean secondary flow,

[4]Hereafter, the ducts with $b/a = 0.67$ and $b/a = 0.5$ are referred to as "wide" and "narrow", respectively.

[5]In this paper, all time-averaged statistics are obtained by using averaging over the four quadrants.

Run	EP2	EP5
C_f	0.00917	0.00908
$\Delta(C_f)$	2.1%	1.0%
U_c/U_b	1.29	1.28
U_c^+	19.00	18.96
$\max\sqrt{U_x^2 + U_y^2}/U_b$	0.0104	0.0135
$\max\|\mathbf{u}'\|_{rms}/U_b$	0.195	0.197

Table 2: Elliptical duct runs: global characteristics

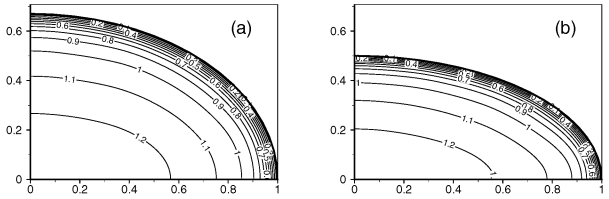

Figure 1: Contours of U_z; (a) - EP2, (b) - EP5.

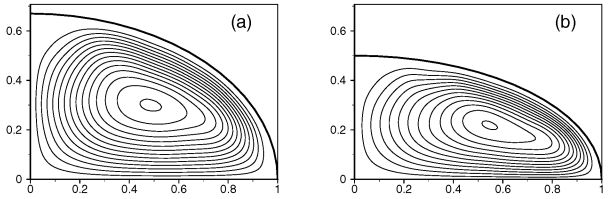

Figure 2: Mean secondary flow contours; (a) - EP2, (b) - EP5.

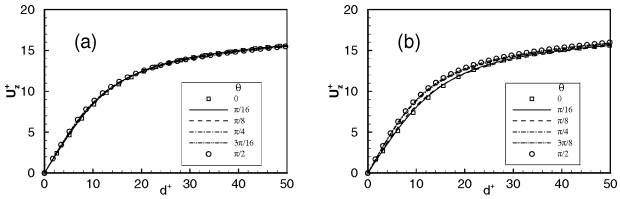

Figure 3: Mean streamwise velocity distribution along the lines perpendicular to the wall; (a) - EP2, (b) - EP5.

which develops in non-circular ducts, affect the cross-sectional distribution of the mean streamwise velocity. The cross-flow streamlines of a secondary flow coincide with the contours of the stream function $\psi(x, y)$ defined by $U_x = \partial\psi/\partial y$, $U_y = -\partial\psi/\partial x$ (U_x and U_y are the cross-stream components of the mean velocity vector). Figure 2 shows the streamlines of the secondary flows which appear as two pairs of counter-rotating vortices[6]. The secondary vortices transfer low-momentum fluid toward the pipe center along the minor principal axis of the ellipse. Vice versa, the high-momentum fluid moves towards the wall along the major axis.

Figure 3a shows that the streamwise velocity U_z profile, normalized by the mean shear velocity, is nearly azimuthal symmetric. For a narrow elliptical pipe, figure 3(b) shows that the velocity distributions along the principal axes are different, but the profiles along the radiuses with $\theta = \pi/4$ and $3\pi/8$ and that along the minor axis practically coincide. This suggests that the mean streamwise velocity is universal for

[6]Figure 2 shows a secondary flow in the first quadrant. A similar distribution is seen in the remaining three quadrants.

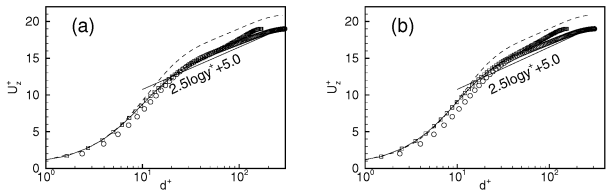

Figure 4: Mean streamwise velocity logarithmic profile along the minor (open circles) and major (squares) axes; dashed line - scaling on the local shear velocity. (a) - EP2, (b) - EP5.

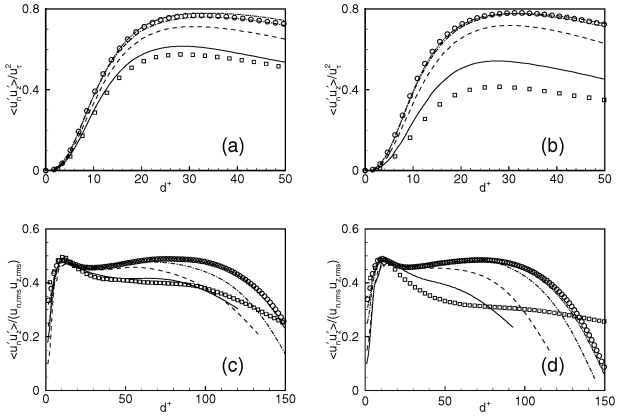

Figure 5: The Reynolds stress (a, b) and correlation coefficient (c, d) of u'_z and u'_n; (a, c) - EP2, (b, d) - EP5. For legend see figure 3

$\pi/4 \le \theta \le \pi/2$, where the wall curvature is much less than for $0 \le \theta \le \pi/8$. To verify this, in figure 4 the logarithmic plots of the streamwise velocity U_z scaled with the mean shear velocity are shown along the minor and major axes. For a wide elliptical pipe (figure 4a), both profiles practically coincide over the interval $20 < d^+ < 100$, indicating very pronounced logarithmic profile. For a narrow pipe, the profiles in figure 4(b) show logarithmic regions with different slopes. In addition, the velocity distribution along the major axis exhibits a linear profile $U_z^+ = d^+$ over $0 \le d^+ \le 10$, which is wider than that observed in turbulent pipes and channels. This suggests that possible flow laminarization took place in the vicinity of the major axis endpoints, a point which deserves further comments. Figure 5 shows the Reynolds shear stress $\langle u'_n u'_z \rangle$ distributions scaled with the mean shear velocity u_τ and the correlation coefficient $\langle u'_n u'_z \rangle / (u_{n,rms} u_{z,rms})$. The subscript n stands for the outward-pointing normal direction to the wall. Therefore, $\langle u'_n u'_z \rangle \equiv \langle u'_x u'_z \rangle$ and $\langle u'_y u'_z \rangle$ for $\theta = 0$ and $\pi/2$, respectively. According to figure 5, it can be seen that there is good agreement between the Reynolds shear stress profiles for $\theta = \pi/4,\ 3\pi/8$ and $\pi/2$ with those in a circular pipe. This means that in the region $\pi/4 < \theta < \pi/2$, the Reynolds stresses are not affected by the wall curvature and therefore the mean wall shear $\overline{\tau}_w$ is a correct scale.

Figures 6–7 show the turbulent intensities normalized by the wall shear velocity. The plots clearly show the suppression of turbulence along the major axis. For a circular pipe, Eggels et al. (1994) discussed the transverse curvature effect as a possible mechanism of turbulence suppression, when

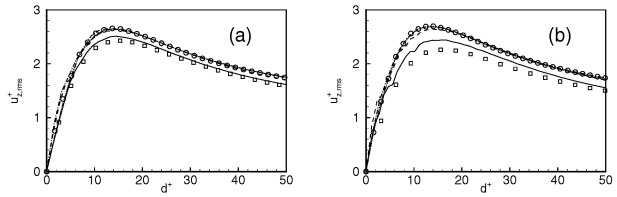

Figure 6: Normalized turbulence intensities near the wall, $u_{z,rms}/u_\tau$. For legend see Fig. 3.

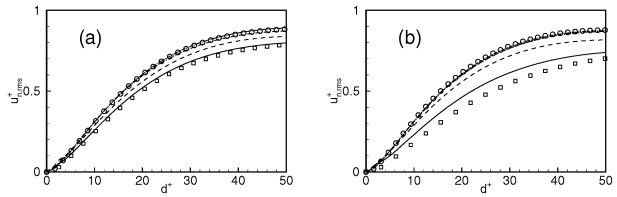

Figure 7: Normalized turbulence intensities near the wall, $u_{n,rms}/u_\tau$. For legend see Fig. 3.

the sweep events[7] are inhibited due to the transverse curvature. For an elliptical pipe, the transverse curvature effect is more significant leading to considerable reduction of turbulence intensities along a major axis. The distribution of the correlation coefficient $\langle u'_n u'_z \rangle / (u_{n,rms} u_{z,rms})$ along minor and major axes, presented in figures $5(c, d)$, exhibits considerable differences for $d^+ > 20$. Notwithstanding that the Reynolds shear stresses $\langle u'_x u'_z \rangle$ measured along the major axis (figure 5) are considerably lower than those observed in pipe and channel turbulent flow, the streamwise velocity profile is in good agreement with the velocity universal logarithmic law (figure 4). In endeavor to understand that, we write the equation for the mean streamwise velocity

$$\overbrace{U_x \frac{\partial U_z}{\partial x} + \frac{\partial \langle u'_x u'_z \rangle}{\partial x}} + \overbrace{U_y \frac{\partial U_z}{\partial y} + \frac{\partial \langle u'_y u'_z \rangle}{\partial y}}$$

$$= \frac{\Delta p}{\rho L_z} + \nu \left(\frac{\partial^2 U_z}{\partial x^2} + \frac{\partial^2 U_z}{\partial y^2} \right). \qquad (8)$$

This is the standard Reynolds-averaged Navier–Stokes equation for the streamwise force-momentum balance, where the first and third terms describe the contribution of the cross-stream secondary flow. Each of the four terms of the left-hand side of (8) represents a different mechanism of the streamwise momentum fluxes. The cross-stream turbulent and secondary flow momentum transport result in redistribution of the streamwise velocity. To observe the influence of each of these mechanisms, we performed the following numerical experiment. For the given U_x, U_y, $\langle u'_x u'_z \rangle$, $\langle u'_y u'_z \rangle$ fields, U_z-velocity field was obtained from (8) with only the secondary flow transport (i.e., the second and the fourth terms are omitted) or, vice versa, only with the turbulent transport (i.e., the first and the third terms are omitted). In both simulations, the pressure drop Δp in (8) corresponds to the turbulent flow with $Re_{D_h} = 6000$. Figure 8 shows the results of this numerical experiment for a narrow pipe, where

[7] Carrying of high-speed fluid towards the wall followed by the energy transfer to the longitudinal and circumferential components

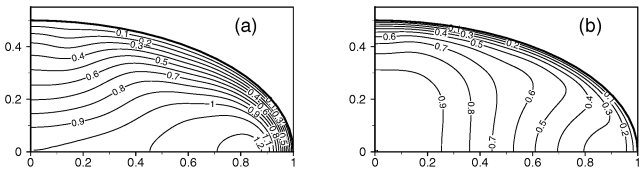

Figure 8: U_z-velocity contours. (a) - "only-secondary flow", (b) - "no-secondary flow".

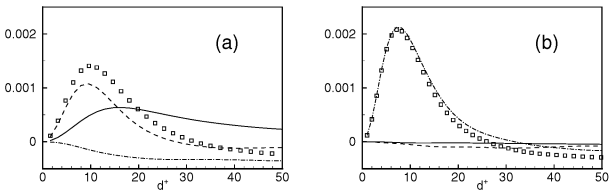

Figure 9: Balance of terms in U_z-equation (8) along the axes; (a) - major axis, $U_y = 0$, solid line - $U_x \partial U_z/\partial x$, (b) - minor axis, $U_x = 0$, solid line - $U_y \partial U_z/\partial y$; (a) and (b): dashed - $\partial\langle u'_x u'_z\rangle/\partial x$, dot-dashed - $\partial\langle u'_y u'_z\rangle/\partial y$, squares - all terms.

the streamwise velocity field normalized by the centerline velocity is shown. From figures $8(a,b)$, we can see that these mechanisms play, apparently, opposite roles. In both cases, the resulting velocity field differs considerably from the actual velocity distribution presented in figure $1(b)$. From figures $1(b)$ and $8(b)$, the "no-secondary flow" field almost does not affect the isovels' patterns in the near-wall region for $\pi/4 \le \theta \le \pi/2$, but changes the flow along the major axis, transferring the low-momentum fluid towards the center. On the contrary, according to figures $1(b)$ and $8(a)$, the "only-secondary flow" significantly changes the isovels' pattern transferring the high-momentum fluid towards the wall along the major axis and the low-speed fluid towards the center along the minor axis.

For comparison, figure 9 shows the terms of (8) in the near-wall region for a narrow pipe. The momentum transport along the major axis is described by the first two terms in (8), where the first term represents the convection of the mean streamwise high-momentum fluid towards the wall. From figure $9(a)$, the first two terms in (8) are of the same order of magnitude, which indicates that the secondary flow along the major axis contributes significantly to the total balance. When we compare the turbulent fluxes of momentum, $\partial\langle u'_x u'_z\rangle/\partial x$ in figure $9(a)$ to $\partial\langle u'_y u'_z\rangle/\partial y$ in figure $9(b)$, we can see that the reduced turbulent flux along the major axis is compensated by the induced secondary flow. This might explain why the velocity profile along the major axis replicates the universal logarithmic profile. The third and the forth terms in (8) represent the momentum transport along the minor axis towards the center. According to figure $9(b)$, the low-momentum fluid transport along the minor axis by the secondary flow is negligibly small. In the near-wall region $0 \le d^+ \le 10$, the total contribution of the momentum transport along the major axis came out to be much less than that along the minor axis. This reduction results in the linear profile $U_z^+ = d^+$.

The elongated "streaks" of alternating low- and high-speed fluid generated near the wall are a noteworthy feature of wall-bounded flows. It is commonly held that the near-wall streaks have a crucial role in turbulence production. The

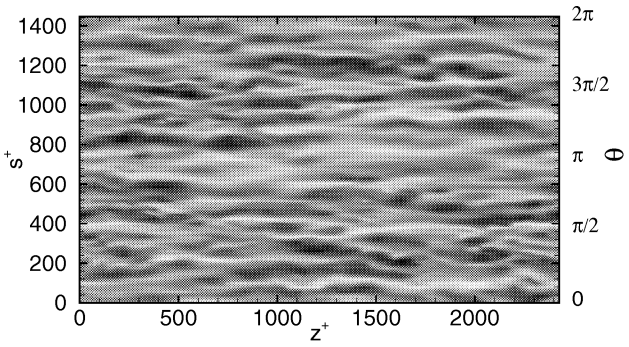

Figure 10: Streaks, $d^+ = 10$, EP5.

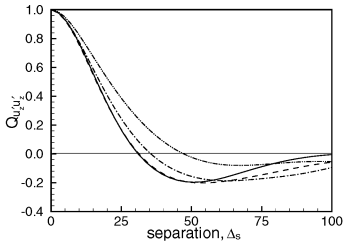

Figure 11: Correlation function $Q_{u'_z u'_z}$; solid line - $d^+ = 10$, dashed line - $d^+ = 20$, dot-dashed line - $d^+ = 30$, dot-dot-dashed line - $d^+ = 50$.

mean spacing between the streaks in the near-wall region is usually obtained from the two-point autocorrelation function of the streamwise velocity with separations in the spanwise (in our case, azimuthal) direction, $Q_{u'_z u'_z}(\Delta_s)$. It is well-accepted that the half mean streak spacing is the separation Δ_s where the minimum (negative) value of $Q_{u'_z u'_z}$ is reached. The spanwise spacing between the streaks for a channel flow is $\lambda^+ \simeq 80 \div 120$ in wall units for moderate Reynolds number flows. Contours of the streamwise velocity component at the circumferential surface distanced at $d^+ = 10$ to the wall are plotted in figure 10. Dark and light colors mark high- and low-speed streaks corresponding to $u'_z > 0$ and $u'_z < 0$, respectively. In the vicinity of the major axis endpoints (marked by $\theta = 0, \pi, 2\pi$), the streaks are less pronounced which is indicative of turbulence attenuation by the transverse curvature effect (figure 10). Figure 11 shows the two-point spanwise (azimuthal) autocorrelation function $Q_{u'_z u'_z}(\Delta_s)$ for different d^+. As can be observed, the estimating the mean streak spacing yields $\lambda^+ \simeq 100$.

SUMMARY

Fully developed turbulent flows in non-circular ducts seem relatively simple as they are unidirectional, but they are actually quite complicated because secondary mean motions develop in the cross-stream plane. These motions are driven by generated mean streamwise vorticity due to the anisotropy of the cross-stream Reynolds stresses. They are an intrinsic feature of turbulent flow in non-circular ducts and play a significant role by cross-stream transferring momentum, heat and mass. An accurate prediction of secondary flows is still difficult for existing turbulent closure models owing to the lack of

comprehensive experimental data. Reported DNS-based data on secondary flows have been restricted to the case of a duct with a square cross-section.

We considered ducts with an elliptic cross-section. Although an elliptical duct is simply a modification of the classic circular pipe, it incorporates the main features of flows in non-circular ducts. To validate the numerical procedure, DNS of turbulent flows through a circular pipe has been carried out. The results showed good agreement with experimental findings and numerical results reported in the literature. Two elliptical ducts were considered with $b/a = 0.67$ and $b/a = 0.5$ (a and b are the ellipse's principal radiuses). The Reynolds number was set to $Re_{D_h} = 6000$, based on hydraulic diameter D_h and bulk flow velocity. The mean streamwise velocity profiles and the turbulence statistics were in good agreement with the known near-wall turbulent characteristics. Cross-stream secondary motions are exhibited by two pairs of vortices which transfer low-momentum fluid towards the duct center along the minor axis. Vice versa, the high-momentum fluid moves toward the wall along the major axis. The maximum intensity of the secondary flows was found to be 1% and 1.4% of bulk velocity for wide and narrow ducts, respectively. Despite this small value, secondary flows play a role comparable with Reynolds stresses for developing the mean velocity profile.

The mean flow characteristics, the Reynolds stresses and turbulence intensities along the minor axis of the elliptical cross-section were found to be similar to plane channel data. The turbulent statistics computed along the major axis is inhibited by the secondary flow transferring high-momentum fluid from the duct's center towards the wall.

The near-wall distributions of turbulence intensities were studied in detail and showed the significant reduction of turbulent activity in the near-wall region of the major axis endpoints. Moreover, the instantaneous velocity fields in the near-wall region revealed structures similar to the "streaks", except in the vicinity of the major axis endpoints. This can be attributed to sweep events of carrying high-speed fluid towards the wall, which are inhibited by the wall transverse curvature effect.

ACKNOWLEDGEMENTS

This research was supported by The Israel Science Foundation Grant 159/02 and in part by the CAER of The Hebrew University of Jerusalem. The work of N.N. was also supported by The Russian Foundation for Basic Research under Grant 02-01-00492.

REFERENCES

Balaras, E., 2004, "Modeling complex boundaries using an external force field on fixed Cartesian grids in large-eddy simulations", *Computers and Fluids*, Vol. 33, pp. 375-404.

Cain, D., and Duffy, J., 1971, "An experimental investigation of turbulent flow in elliptical ducts", *International Journal of Mechanical Sciences*, Vol. 13, pp. 451-459.

Demuren, A. O., and Rodi, W., 1984, "Calculation of turbulence-driven secondary motion in non-circular ducts", *Journal of Fluid Mechanics*, Vol. 140, pp. 189-222.

Eggels, J. G. M., Unger, F., Weiss, M. H., Westerweel, J., Adrian, R. J., Friedrich, R., and Nieuwstadt, F. T. M., 1994, "Fully developed turbulent pipe flow: a comparison between direct numerical simulation and experiment", *Journal of Fluid Mechanics*, Vol. 268, pp. 175-209.

Fadlun, E. A., Verzicco, R., Orlandi, P., and Mohd-Yusof, J., 2000, "Combined immersed-boundary finite-difference methods for three-dimensional complex flow simulations", *Journal of Computational Physics*, Vol. 161, pp. 35-66.

Gavrilakis, S., 1992, "Numerical simulation of low-Reynolds-number turbulent flow through a straight square duct", *Journal of Fluid Mechanics*, Vol. 244, pp. 101-129.

Huser, A., and Biringen, S., 1993, "Direct numerical simulation of turbulent flow in a square duct", *Journal of Fluid Mechanics*, Vol. 257, pp. 65-95.

Kim, J., Kim, D., and Choi, H., 2001, "An immersed-boundary finite-volume method for simulations of flow in complex geometries", *Journal of Computational Physics*, Vol. 171, pp. 132-150.

Madabhushi, R.K., and Vanka, S.P., 1993, "Direct numerical simulations of turbulent flow in a square duct at low Reynolds number", in: So, R. M. C., Speziale, C. G., Launder, B. E. (Eds.), *Near-Wall Turbulent Flows*, Elsevier, pp. 297-306.

Mohd-Yusof, J., 1997, "Combined immersed boundaries/B-splines method for simulations of flows in complex geometries", *CTR Annual Research Briefs*, NASA Ames/Stanford University.

Moin, P., and Mahesh, K., 1998, "Direct numerical simulation: a tool in turbulence research", *Annual Review of Fluid Mechanics*, Vol. 30, pp. 539-578.

Moin, P., 2002, "Advances in large eddy simulation methodology for complex flows", *International Journal of Heat and Fluid Flow*, Vol. 23, pp. 710-720.

Nikitin, N., 1994, "Direct numerical modelling of three-dimensional turbulent flows in pipes of circular cross section", *Fluid Dynamics*, Vol. 29, pp. 749-757.

Nikitin, N., 1996, "Statistical characteristics of wall turbulence", *Fluid Dynamics*, Vol. 31, pp. 361-370.

Nikitin, N, 1997, "Numerical simulation of turbulent flows in a pipe of square cross section", *Physics-Doklady*, Vol. 42, pp. 158-162.

Peskin, C. S., 1972, "Flow patterns around heart valves: a numerical method", *Journal of Computational Physics*, Vol. 10, pp. 252-271.

Rai, M. M., and Moin, P., 1991, "Direct simulations of turbulent flow using finite-difference schemes", *Journal of Computational Physics*, Vol. 96, pp. 15-53.

Swarztrauber, P. N., 1974, "A direct method for the discrete solution of separable elliptic equations", *SIAM Journal on Numerical Analysis*, Vol. 11, pp. 1136-1150.